Removing the Effect of Lunar Topography on Mini-RF SAR Polarimetric Parameters Through DEM Data

Zhanchi Huang, Zhaobo Song, Gaofeng Shu, *Member, IEEE*, Yabo Huang, and Ning Li, *Member, IEEE*

***Abstract*— Topography exerts a significant influence on the polarimetric parameters of synthetic aperture radar (SAR), making its study crucial for advancing scientific research. Accurate analysis of topography-independent content requires the removal of lunar topography effects. This letter presents a statistical-based method for assessing the impact of topography on SAR images. It involves the calculation of various SAR parameters and local incidence angle (LIA) using Lunar Reconnaissance Orbiter's (LRO) Mini-RF SAR and Lunar Orbiter Laser Altimeter (LOLA) digital elevation model (DEM) data, respectively. By establishing a mapping relationship between LIA and SAR parameters through coregistration, the proposed method enables an insightful examination of topography effects. The method is applied to analyze and mitigate topography influences on lunar SAR images acquired by Mini-RF, indicating that LIA has a pronounced effect on SAR parameters in relatively flat areas, while its correlation weakens in rougher regions. This analysis provides valuable insights for classifying lunar regolith based on the effects of topography on SAR images.**

***Index Terms*— Digital elevation model (DEM), Lunar Reconnaissance Orbiter's (LRO), Mini-RF, Stokes parameters, synthetic aperture radar (SAR), topography.**

I. Introduction

SYNTHETIC aperture radar (SAR) is an active remote sensing system, which has been widely used in various fields. According to the characteristics of SAR imaging, SAR images contain a large amount of geometry and material information of the observed area [1]. Researches show that the topography of the surface is one of the main factors that contribute to SAR echo intensity [2].

The lunar surface is covered by thick regolith without vegetation, buildings, rivers, etc. The average value of the lunar regolith is about 5 m at maria and 12 m at highland [3], [4]. At present, Mini-RF SAR data can be used to study various aspects of the lunar surface such as dielectric constant, water ice, and rock abundance [5], [6], [7], which shows the great application potential in lunar scientific mission. SAR image itself contains coupled information, including lunar topography, dielectric constant, surface roughness, etc.

Manuscript received 18 July 2023; revised 24 September 2023 and 25 November 2023; accepted 12 December 2023. Date of publication 14 December 2023; date of current version 21 December 2023. This work was supported by the Natural Science Foundation of Henan under Grant 222300420115. *(Corresponding author: Gaofeng Shu.)*

The authors are with the College of Computer and Information Engineering, the Henan Key Laboratory of Big Data Analysis and Processing, and the Henan Province Engineering Research Center of Spatial Information Processing, Henan University, Kaifeng 475004, China (e-mail: gaofeng.shu@henu.edu.cn).

Digital Object Identifier 10.1109/LGRS.2023.3343116

TABLE I
PARAMETERS OF LRO MINI-RF AND LOLA DEM

Parameters	Unit	LRO Mini-RF	LOLA DEM
Incidence Angle	Degree	52.1638	N/A
Wavelength	cm	12.6	N/A
Map scale	m/pixel	14.8	59.2253
Product Id	N/A	lsz_01422_1cd_xku_10n342_v1	sldem2015_512_00n_30n_315_360_float

It is essential to consider the effect of topography on SAR parameters as it can significantly affect the calibration of SAR parameters [2]. However, it is quite challenging to decouple different factors due to the complexity of SAR imaging mechanisms. Hajnsek et al. [8] used the Bragg scattering model to establish a correlation between the scattering matrix and factors, i.e., target roughness, complex relative permittivity, and local incidence angle (LIA). However, this model necessitates fully polarimetric SAR data. In addition, Evans et al. [9] used empirical formulas to represent the relationship between LIA and SAR backscatter intensity. However, it cannot reveal the relationship between LIA and other decomposed polarimetric parameters.

In this letter, a method that decouples and analyzes the effect of lunar topography on decomposed compact polarimetric parameters of Mini-RF data is proposed. First, the LIA image is obtained through Lunar Orbiter Laser Altimeter (LOLA) digital elevation model (DEM) data. Second, the LIA image and the Mini-RF SAR parameters' image are coregistered to establish the relationship between them by a statistic method. Finally, the topography is decoupled from other factors, and the effect of that on the SAR parameters is analyzed.

The rest of this letter is organized as follows. Section II presents the data and method that reveals the relationship between LIA and SAR parameters. Section III presents the detail of the experiment and results. Section IV presents the analysis and discussion. Section V presents the conclusion.

II. Data and Method

The parameters of Mini-RF data and DEM data used in this letter are shown in Table I.

A. LIA Calculation

In this letter, the DEM data are used to calculate LIA. An arbitrary plane in the Cartesian coordinate system, as shown in Fig. 1, is constructed as

$$ax + by + cz + d = 0 \tag{1}$$

where a, b, c, d are the coefficients of the plane equation.

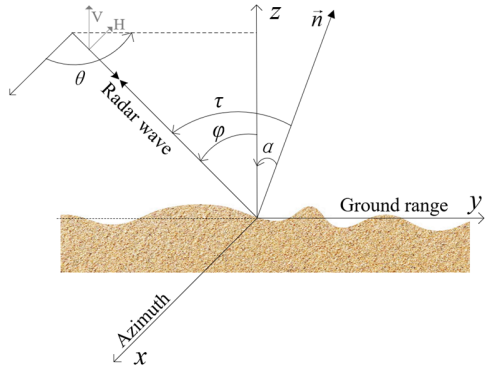

Fig. 1. Geometry of SAR imaging parameters. $\vec{n}$ is the normal to a plane determined by the DEM data. α is the angle between the normal and the $+z$-axis. φ is the angle between the reversed unit direction vector of radar line of sight and $+z$-axis, i.e., the global incidence angle. τ is the angle between the reversed unit direction vector of radar line of sight and $\vec{n}$, i.e., the LIA.

In this letter, the adjacent 3×3 points of DEM data are chosen to estimate the normal vector to the plane $\vec{n} = (a, b, c)$. For the case of the lunar surface, α should satisfy $0 \le \alpha \le \pi/2$, i.e., $c \ge 0$.

Each point of the 3×3 frame's points has three values (x_{ij}, y_{ij}, z_{ij}), $i, j \in \{-1, 0, 1\}$, where z_{ij} value is the elevation.

There are four unknown parameters to be determined while nine samples were selected, so the least-square method is chosen to estimate these parameters, i.e.,

$$\begin{aligned} &\min_{a,b,c,d} \sum_{i=-1}^{1} \sum_{j=-1}^{1} \left(ax_{ij} + by_{ij} + cz_{ij} + d\right)^2 \\ &\text{s.t. } a^2 + b^2 + c^2 = 1 \\ &\quad c > 0. \end{aligned} \tag{2}$$

The estimated unit normal vector $\hat{n} = (\tilde{a}, \tilde{b}, \tilde{c})$. Let the reversed unit direction vector of the radar line of sight be $\hat{n}_r = (0, -\sin\varphi, \cos\varphi)$. The LIA τ is derived as

$$\cos\tau = \hat{n} \cdot \hat{n}_r = -\tilde{b} \cdot \sin\varphi + \tilde{c} \cdot \cos\varphi \tag{3}$$

where $0 \le \tau \le \pi/2$. $\tau > \pi/2$ is ignored in this letter because electromagnetic waves cannot reach the region.

B. SAR Parameters' Calculation

The SAR data used in this letter are given in the form of Stokes parameters, and the calculation method of these parameters is described below.

1) Stokes Parameters: The Stokes parameters consist of four components

$$\begin{bmatrix} I_1 \\ I_2 \\ I_3 \\ I_4 \end{bmatrix} = \begin{bmatrix} \langle |E_{HL}|^2 + |E_{VL}|^2 \rangle \\ \langle |E_{HL}|^2 - |E_{VL}|^2 \rangle \\ 2\mathrm{Re}\langle E_{HL} E_{VL}^* \rangle \\ -2\,\mathrm{Im}\langle E_{HL} E_{VL}^* \rangle \end{bmatrix} \tag{4}$$

where I_1 denotes the total power of both the horizontal and vertical components, I_2 denotes the difference power between the horizontal and vertical components, and I_3 and I_4 denote the parts of the two opposite circular polarizations, respectively [5].

2) m-χ Decomposition: The m-χ decomposition can be used to decompose the Stokes parameters into the single-scattering s, double-scattering d, and volume scattering v components

$$\begin{bmatrix} s \\ v \\ d \end{bmatrix} = \sqrt{I_1} \cdot \begin{bmatrix} \sqrt{\dfrac{m(1-\sin 2\chi)}{2}} \\ \sqrt{1-m} \\ \sqrt{\dfrac{m(1+\sin 2\chi)}{2}} \end{bmatrix} \tag{5}$$

where

$$\begin{aligned} m &= \left(\sqrt{I_2^2 + I_3^2 + I_4^2}\right) \Big/ I_1 \\ \sin 2\chi &= I_4/(mI_1) \end{aligned} \tag{6}$$

where m is the degree of polarization of the Stokes vector, and χ is the ellipticity angle of the Stokes vector.

3) Circular Polarization Ratio (CPR): In this letter, the CPR is calculated as follows [5]:

$$\mathrm{CPR} = \frac{I_1 - I_4}{I_1 + I_4}. \tag{7}$$

C. Establish the Relationship Between SAR Parameters and LIA

The intensity of the SAR parameter is a function of continuous variables, including the LIA, which is described as follows [8]:

$$\begin{aligned} \sigma &= 8k^4\delta^2 \cos^4\tau |f|^2 W(2k\sin\tau, 0) \\ f &= (\varepsilon_r - 1) \frac{\sin^2\tau - \varepsilon_r\left(1 + \sin^2\tau\right)}{\left[\varepsilon_r \cos\tau + \left(\varepsilon_r - \sin^2\tau\right)^{\frac{1}{2}}\right]^2} \end{aligned} \tag{8}$$

where σ represents the intensity of the SAR parameters. τ represents the incident angle, and δ and ε_r are the roughness and dielectric constant, respectively. k and $W(\cdot)$ are the wavenumber and roughness spectrum of the surface respectively.

The function $W(2k\sin\tau, 0)$, which is a function of both τ and k, can be regarded solely as a function of τ, given the limited range of k variations attributable to the relatively narrow bandwidth (8 MHz) of Mini-RF within its operational frequency (2.38 GHz).

The function f, which is a function of both ε_r and τ, can also be regarded solely as a function of τ. The range of ε_r is $1 < \varepsilon_r < 10$ [5]. However, in a smaller lunar surface area, the dielectric constant ε_r exhibits only minor variations within a limited range. Consequently, in this scenario, f can be considered as a function solely dependent on τ.

Let

$$f(\delta) = 8k^4\delta^2, \quad g(\tau) = \cos^4\tau |f_{VV}|^2 W(2k\sin\tau, 0). \tag{9}$$

Then

$$\sigma = f(\delta) \cdot g(\tau). \tag{10}$$

Given a random distribution of samples of (10) (τ, σ). Assuming that noise n functions $f(\delta)$ and $g(\tau)$ satisfy specific distributions on the same image, let μ_n represent the mean value of noise. Dividing the LIA value τ into N intervals, the lth interval satisfies

$$(l-1) \cdot t \le \tau_l < l \cdot t, \quad l = 1, 2, 3, \ldots, N \tag{11}$$

where t represents the interval length.

For a specific SAR image, each pixel has a corresponding LIA, which means there is finite LIA for a specific image. Let the pth value of the lth interval be as follows:

$$\sigma_{lp} = f\left(\delta_{lp}\right) \cdot g\left(\tau_{lp}\right) + n_{lp}. \tag{12}$$

The average of each interval can be expressed as

$$\bar{\sigma}_l = \frac{1}{N_k}\sum_{p=1}^{N_k} f_1\left(\tau_{lp}\right) \cdot g(\tau_l) + \frac{1}{N_k}\sum_{p=1}^{N_k} n_{lp} \tag{13}$$

where $\overline{\sigma_l}$ represents the average of the SAR intensity of the lth interval. N_k represents the total elements of the lth interval.

Since it is assumed that the noise is independent of τ, its mean value in any interval is the same as the global mean value. And f is a continuous function, when N_k is big enough and t is small enough, (13) can be written as

$$\bar{\sigma}_l = \overline{f(\delta_l)} \cdot g(\tau_l) + \mu_n \tag{14}$$

where $\overline{f(\delta_l)}$ represents the average of the function f of the lth interval. Equation (13) shows the relationship between the SAR parameters and the LIA of the lth interval.

D. Removing and Evaluating the Effect of Topography

Subtract (14) from (12) and then divide (14)

$$\frac{\sigma_{lp} - \bar{\sigma}_l}{\bar{\sigma}_l} = \frac{f\left(\delta_{lp}\right) - \overline{f(\delta_l)}}{\overline{f(\delta_l)}} + \mu_n' \tag{15}$$

where μ_n' represents the new average value of noise.

Formula (15) is independent of τ which means $(\sigma_{lp} - \bar{\sigma}_l)/\bar{\sigma}_l$ is independent of the topography.

To evaluate the results, using the first-order linear curve to fit the derived relationship of LIA and SAR parameters, the linear gradient was used to represent the relationship of LIA and SAR parameters. For a given SAR parameter, the more it is near 0, the more independent it is with LIA. And the Pearson correlation coefficient was used to represent the degree of correlation between LIA and SAR parameters.

The flowchart of the proposed method is shown in Fig. 2. In this letter, control points were selected based on crater edge and center features, and interpolation was performed using the mapping relationships between these control points.

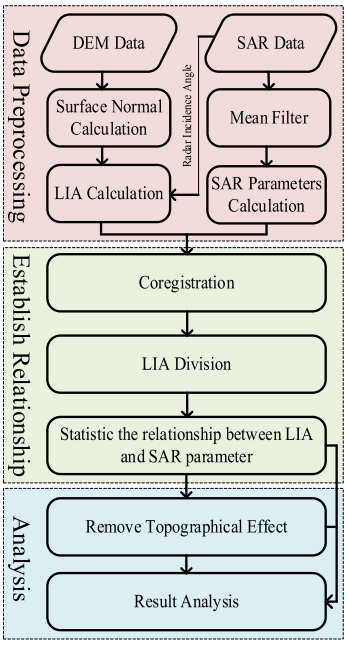

Fig. 2. Flowchart of the proposed method.

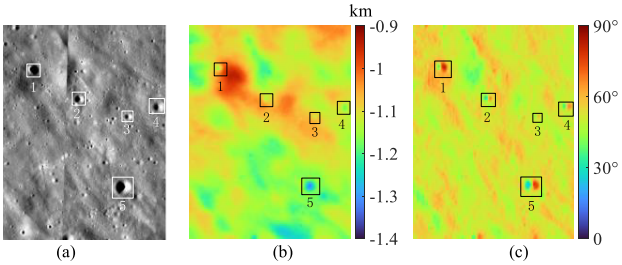

Fig. 3. (a) Optical image. (b) LOLA DEM image. (c) LIA derived from surface normal and SAR incidence angle.

TABLE II
STATISTIC VALUES OF FIG. 3

Figure	minimum	average	maximum
Fig. 3(b)	−1.3192 km	−1.1204 km	−0.9439 km
Fig. 3(c)	24.6442°	52.2676°	81.6930°

(The value of Fig. 3(b) is relative to a radius of 1737.4 km.)

III. APPLICATION OF THE PROPOSED METHOD

To validate the efficacy of the proposed method, a lunar region with diverse topography was chosen. Fig. 3 illustrates the optical image, original DEM, and derived LIA. The numbered rectangles in Fig. 3 correspond to five craters. Notably, the identification of crater features is more discernible in the LIA image compared with the DEM image of identical resolution.

Table II presents the statistic values of Fig. 3(b) and (c), which shows a diverse topography of the selected area.

Fig. 4 presents the images obtained from the Stokes parameters. Analysis of the images reveals that I_1, I_2, I_3, I_4, s, v, and d exhibit prominent topographical characteristics. Conversely, the CPR displays less correlation with the topography features.

Fig. 5 shows the number of pixels of each LIA interval which is derived from Fig. 3(c). It shows that the pixels are mainly concentrated in 40°–65°. Fig. 6 shows the relationship of the LIA and SAR parameters. Combining Figs. 5 and 6, it can be seen that the curve in Fig. 6 is smooth in 40°–65° of the values of the LIA. The smoothness of the curve indicates the accuracy of the derived relationship. In the interval of 20°–40°, the SAR intensity value is relatively large, but the curve fluctuates due to the limited number of pixels and registration errors between SAR images and LIA images. The curve is relatively stable within 40°–65° and showed a good negative correlation between the LIA and the intensity of SAR parameters. In intervals greater than 65°, the curve becomes no longer stable due to the decrease in the number of pixels, while the overall trend remains decreasing. If more data are used, the proposed method will be more reliable and accurate.

Fig. 7 shows the SAR parameters after removing the effect of lunar topography, i.e., the nontopography information. The resulting images without topography have the potential to classify lunar roughness. Compared with Fig. 4, the topography information in Fig. 7 should be eliminated. However, it is worth noting that certain areas (such as the crater) still

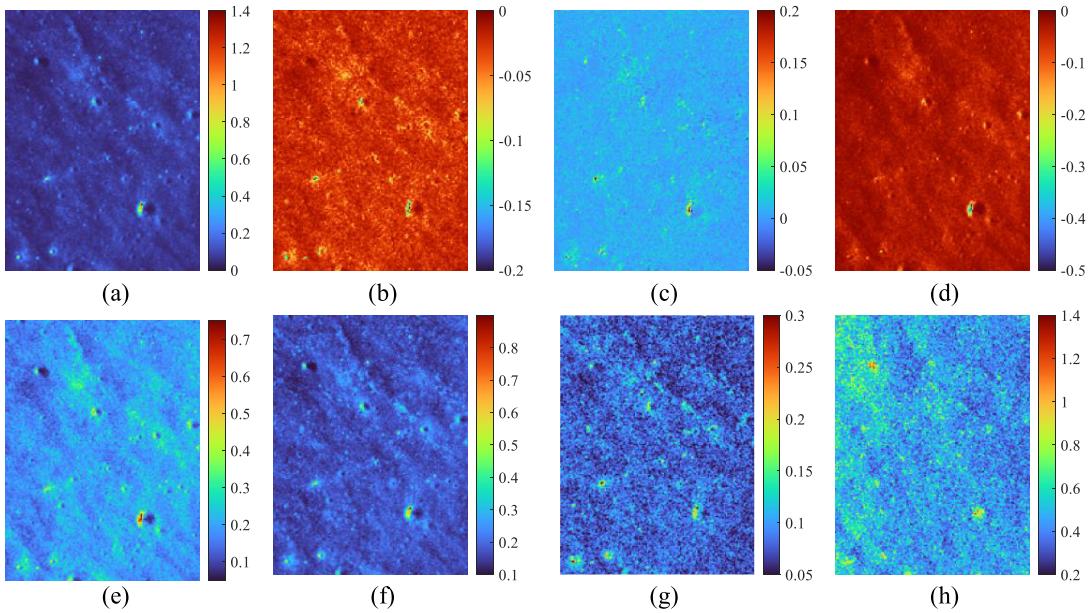

Fig. 4. Original SAR parameters. (a)–(d) Stokes parameters. (e) Single scattering. (f) Volume scattering. (g) Double scattering. (h) CPR.

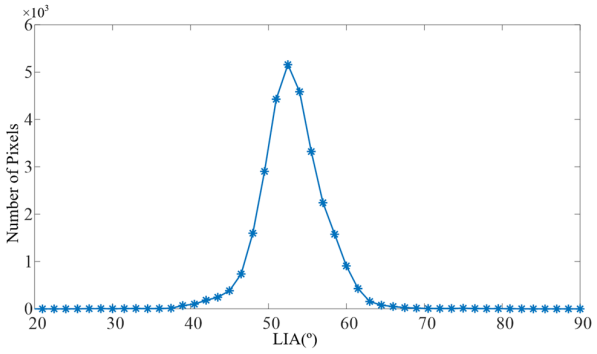

Fig. 5. Number of pixels of each LIA interval.

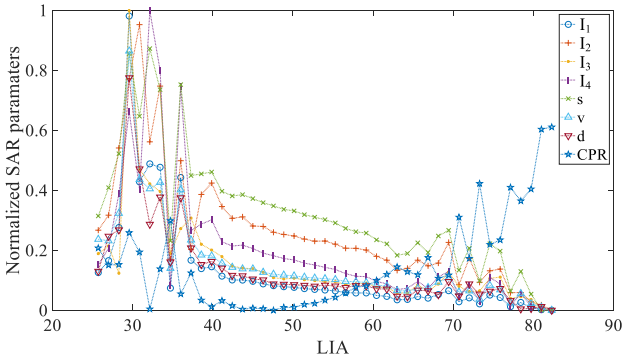

Fig. 6. Statistical average value of SAR parameters versus LIA.

display potential indications of topography. First, this disparity might be attributed to the variations in material composition or surface roughness. Second, the larger and smaller LIAs are mainly distributed in the crater area, resulting in a large error and making the removal of the topography incomplete. Finally, the residual topographic information can be attributed to the low resolution of the DEM data.

Fig. 8(a) shows the linear gradient before and after LIA removal, and Fig. 8(b) shows the Pearson correlation coefficient before and after LIA removal. For a given SAR parameter, linear gradient near 0 indicates that the SAR parameter is less relevant with LIA. Fig. 8 shows that the proposed method can significantly remove the effect of LIA's influence from SAR parameters.

IV. Discussion

In this letter, a method is proposed to decouple and analyze the influence of lunar topography on various SAR parameters of the Mini-RF data using DEM data. The existing literature [10] that investigates the impact of lunar topography on SAR parameters exclusively uses SAR data. However, this letter establishes a correlation between lunar

topography and SAR parameters through the utilization of DEM data. In addition, the influence of topography can be removed using statistical methods. It is important to note two limitations within this letter. First, the resolution of DEM data used is 59.23 m/pixel, which is lower than that of SAR data, resulting in a lower resolution of the extracted LIA and a reduced accuracy of the results. Consequently, despite efforts to eliminate the influence of topography, residual topographic information may still persist within the image. Second, the distribution of extracted LIA is uneven, with a scarcity of both smaller and larger LIAs, leading to substantial error and incomplete topography removal. To ensure enhanced accuracy and efficacy, higher resolution DEM data, SAR data, and SAR satellites with multiple incident angles should be used in the future.

V. Conclusion

SAR images are valuable to conduct scientific research in lunar missions due to their ability to provide rich information. However, these images contain coupled data from various factors, presenting a challenge. An effective approach to overcome this challenge involves decoupling the different factors to assess the specific impact of each factor on SAR parameters. Previous studies [4], [5], [6], [9], [10], [11], [12] focused on the decomposition of just the SAR parameters without introducing new information. To enhance the analysis of the

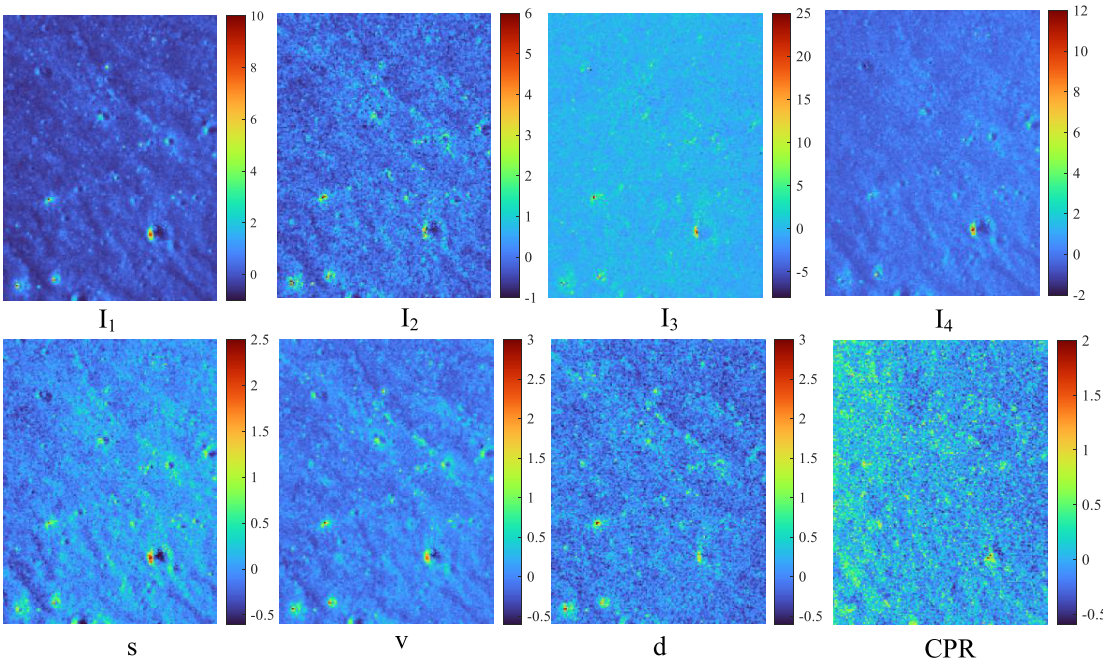

Fig. 7. SAR parameters removed topography.

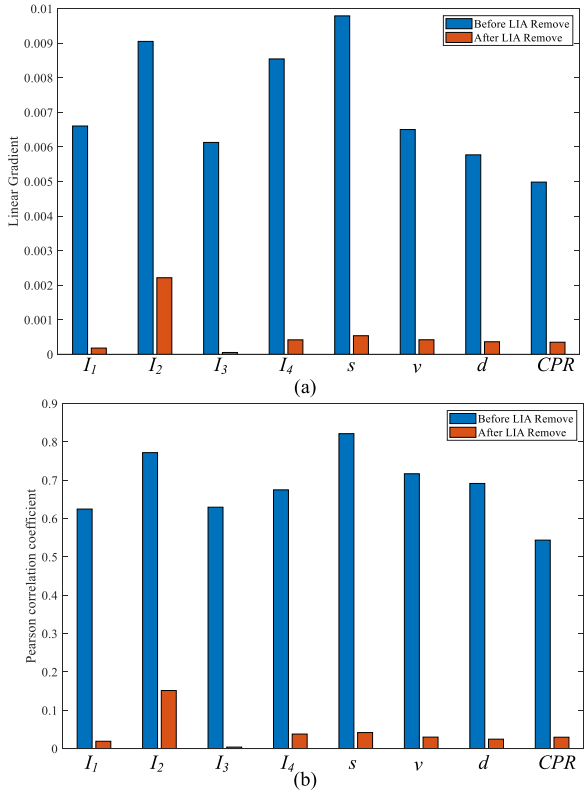

Fig. 8. (a) Linear gradient and (b) Pearson correlation coefficients between SAR parameters and LIA.

particular factor, the incorporation of auxiliary data proves to be beneficial.

In this letter, to analyze the effect of lunar topography on SAR images, LOLA DEM data were incorporated with Mini-RF data to decompose the topographical information based on a statistic method. The result shows that the effect of lunar topography on SAR parameters is generally removed. After removing the effect of topography, the image shows non-topographical information, which hold potential for classifying lunar regolith, consequently.

REFERENCES

[1] G. Di Martino, A. Di Simone, A. Iodice, D. Riccio, and G. Ruello, "Estimation of the local incidence angle map from a single SAR image," in *Proc. ESA Living Planet Symp.*, Aug. 2016, p. 399.

[2] J. J. van Zyl, B. D. Chapman, P. Dubois, and J. Shi, "The effect of topography on SAR calibration," *IEEE Trans. Geosci. Remote Sens.*, vol. 31, no. 5, pp. 1036–1043, Sep. 1993.

[3] W. Fa and Y. Cai, "Circular polarization ratio characteristics of impact craters from mini-RF observations and implications for ice detection at the polar regions of the Moon," *J. Geophys. Res., Planets*, vol. 118, no. 8, pp. 1582–1608, Aug. 2013.

[4] W. Fa and Y.-Q. Jin, "A primary analysis of microwave brightness temperature of lunar surface from Chang-E 1 multi-channel radiometer observation and inversion of regolith layer thickness," *Icarus*, vol. 207, no. 2, pp. 605–615, Jun. 2010.

[5] Y. Gao et al., "Investigating the dielectric properties of lunar surface regolith fines using mini-RF SAR data," *ISPRS J. Photogramm. Remote Sens.*, vol. 197, pp. 56–70, Mar. 2023.

[6] D. Putrevu, A. Das, J. G. Vachhani, S. Trivedi, and T. Misra, "Chandrayaan-2 dual-frequency SAR: Further investigation into lunar water and regolith," *Adv. Space Res.*, vol. 57, no. 2, pp. 627–646, Jan. 2016.

[7] N. Liu and Y.-Q. Jin, "A statistical rule of the Stokes parameters of Pol-SAR for identifying flat surface in PSR," *IEEE Geosci. Remote Sens. Lett.*, vol. 20, pp. 1–5, 2023.

[8] I. Hajnsek, E. Pottier, and S. R. Cloude, "Inversion of surface parameters from polarimetric SAR," *IEEE Trans. Geosci. Remote Sens.*, vol. 41, no. 4, pp. 727–744, Apr. 2003.

[9] D. L. Evans, T. G. Farr, and J. J. van Zyl, "Estimates of surface roughness derived from synthetic aperture radar (SAR) data," *IEEE Trans. Geosci. Remote Sens.*, vol. 30, no. 2, pp. 382–389, Mar. 1992.

[10] N. Liu and Y.-Q. Jin, "Simulation of Pol-SAR imaging and data analysis of mini-RF observation from the lunar surface," *IEEE Trans. Geosci. Remote Sens.*, vol. 60, 2022, Art. no. 2000411.

[11] A. Vashishtha and S. Kumar, "Characterization of geomorphological features of lunar surface using Chandrayaan-1 mini-SAR and LRO mini-RF data," *Quaternary Int.*, vols. 575–576, pp. 338–357, Feb. 2021.

[12] W. Fa, M. A. Wieczorek, and E. Heggy, "Modeling polarimetric radar scattering from the lunar surface: Study on the effect of physical properties of the regolith layer," *J. Geophys. Res.*, vol. 116, no. 3, Mar. 2011.